Archives of Mechanics • Archiwum Mechaniki Stosowanej • 29, 6, pp. 829–846, Warszawa 1977

Plane plastic flow of granular model material Experimental setup and results (*)

M. BECKER (WUPPERTAL) and H. LIPPMANN (MÜNCHEN)

THE CONVENTIONAL tests in soil mechanics do not allow for a rotation of the principal axes of the state of stress. Either a homogeneous stress distribution appears, as for instance in the truly triaxial machine [1, 2], or there results a fracture zone in which the behaviour of the material cannot experimentally be examined, as for instance in the simple shear test [3]. In this investigation large plastic deformations of a granular model material under inhomogeneous stress distribution are studied. Therefore we developed a setup which is sketched in Fig. 1. Using many tests series we examined different yield laws and checked whether the calculated stress values agreed with the measured quantities or not. The experiments show a fairly good agreement, provided that the Coulomb yield criterion in connection with the flow rule of Brown-Gudehus, are employed as constitutive equations.

Doświadczenia konwencjonalne w mechanice ośrodków sypkich nie dopuszczają obrotu głównych osi stanu naprężenia. Otrzymuje się bądź jednorodny stan naprężenia, jak na przykład w prawdziwie trójosiowych aparatach [1, 2], lub powstaje strefa zniszczenia, w której zachowanie się materiału nie jest trudne do zbadania doświadczalnego, jak na przykład w próbach na czyste ścinanie [3]. W niniejszej pracy badane są duże odkształcenia plastyczne modelowego materiału ziarnistego, wywołane niejednorodnym rozkładem stanu naprężenia. W tym celu zbudowaliśmy stanowisko doświadczalne, które pokazane jest schematycznie na rys. 1. Wykonując wiele serii doświadczeń zbadaliśmy różne prawa płynięcia i sprawdziliśmy czy policzone wartości naprężeń są zgodne z mierzonymi wielkościami czy nie. Wyniki doświadczeń wykazują zupełnie dobrą zgodność pod warunkiem, że jako równania konstytutywne przyjmie się warunek plastyczności Coulomba wraz z prawem płynięcia Browna-Gudehusa.

Конвенционные эксперименты в механике сыпучих сред не допускают вращения главных осей напряженного состояния. Получается или однородное напряженное состояние, как например в действительно трехсоных аппаратах [1, 2], или возникает зона разрушения, в которой поведение материала не трудно исследовать экспериментально, как например в испытаниях на чистый сдвиг [3]. В настоящей работе исследуются большие пластические деформации модельного зернистого материала вызванные неоднородным распределением напряженного состояния. С этой целью построена исследовательская установка, которая показана схематически на рис. 1. Проводя много серий экспериментов исследованы разные законы течения и проверено, совпадают или нет, расчитанные значения напряжений с измеренными величинами. Результаты экспериментов показывают совсем хорошее совпадение под условием, что определяющие уравнения принимаются в виде условия пластичности Кулона, совместно с законом течения Броуна-Гудегьюса.

Notations

r θ polar coordinates,

σ_{jk} stress tensor with $\sigma_r = \sigma_{rr} < 0$, $\sigma_\theta = \sigma_{\theta\theta} < 0$, and $\tau = \sigma_{r\theta}$,

σ_p centre of the stress circle (Mohr),

σ_q radius of the stress circle,

(*) Paper presented at the Euromech Colloqium 84 on "Mechanics of Granular Materials", Warsaw, July 1976.

http://rcin.org.pl

s_{jk} deviator stress tensor,
ε_{jk} plastic components of the strain tensor,
ε_p centre of the strain circle (Mohr),
ε_q radius of the strain circle,
e_{jk} plastic components of deviatoric strain tensor,
Ω angular velocity of the inner core,
u radial displacement,
v circumferential displacement,
μ coefficient of Coulomb friction between steel and glass,
ϱ relative density (ratio of the solid particle volume, and the total volume) of the model material,
ϱ_c critical density for which deformation occurs without change of volume)
l length of the steel rodlets,
γ specific weight of the steel rodlets,
α angle between the r-direction and the direction of the first principal stress,
f_σ yield function,
Φ angle of internal friction,
c internal cohesion,
ψ angle between the flow limit and the σ_p-axis in the plane of state,
g function which indicates the change of volume,
D dilatancy function,
β angle of dilatancy,
Ψ_σ potential function different from the yield function f_σ,
$\Delta\lambda$ positive incremental multiplier,
t time,
t_0 initial time,
Δt_m duration of each individual process of registering,
Δt_w time interval between two registerings,
Δ increment,
h_p thickness of the polyurethane plate,
d_p diameter of the polyurethane plate,
p_t gas pressure in the rubber tube,
d_t diameter of the rubber tube,
index i values at the inner boundary,
index e values at the outer boundary.

1. Introduction

IN SOIL mechanics it is usually assumed that:

A1: *The state and the motion of material are completely defined by the classical concept of stress, strain, strain rate, and local density.*

This assumption is not at all trivial. Nevertheless a physical proof is difficult [4]. Indeed it is conceivable that the motion of the set of individual grains is not uniquely determined by the field of average grain displacement. The same is true with respect to the rotations of the grains and the interaction of both. Therefore, there may exist different states of stress which are all associated with the same average field of displacement. This case is excluded by the first assumption. An experimental justification that the grain rotation may be neglected has not yet been given, because the usual setups do not allow for a rotation of the principal axes of the state of stress or of the strain increments respectively, so

http://rcin.org.pl

that the grain rotation is of minor significance from the very beginning. Our experimental investigations should allow for such a justification.

A further assumption which is used occasionally in connection with plastic constitutive equations is the following one:

A2: *The stress path should be independent of the velocity with which the strain path is run.*

Since an exact time independence is physically impossible for natural granular material, a class of ideal material is considered. In fact, the behaviour of dry granular material is governed by internal contact friction between the grains, which is time-independent within a very large area of the velocity [5].

2. The setup

2.1. Preliminary considerations

Instead of grains we have — following the example of SCHNEEBELI [6] — presently chosen steel rodlets two centimetres in lenght, which stand perpendicular to the plane of Fig. 1. This model material — a one-phase material — is deformed between the concentric boundaries r_i and r_e. In this way we enforce plane plastic flow. Since very simple

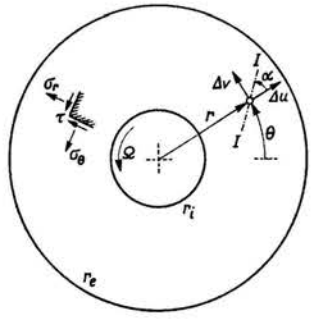

FIG. 1. Schematic diagram of the setup.

preliminary tests show that by a rigid rotation of the inner core only the deformation concentrates to one shear zone alone (Fig. 2) which may become about ten grains thick [7], a core r_i was designed which can be rotated as well as extended. The outer boundary r_e shall be extensible only. If one rotates the inner core r_i and expands it simultaneously, a deformation is imposed on the material which is inhomogeneous with respect to the radius r. But it is independent of the angle θ so that it may be described as being rotationally symmetric rather than axially symmetric.

The construction of these boundaries was the main difficulty of the setup, the more as no literature seems to exist about a circular loading or measuring equipment which can change its diameter continuously.

http://rcin.org.pl

A)

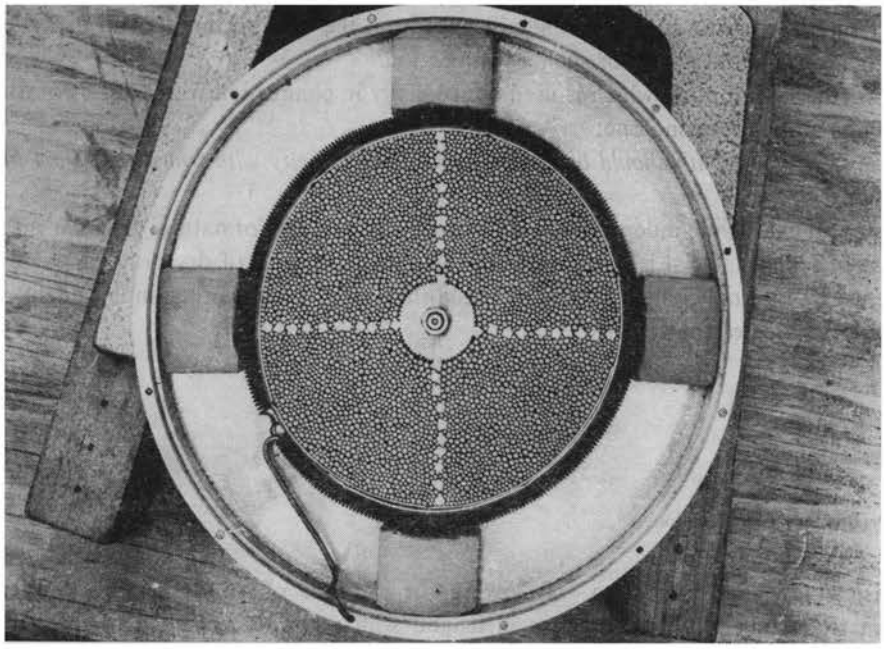

B)

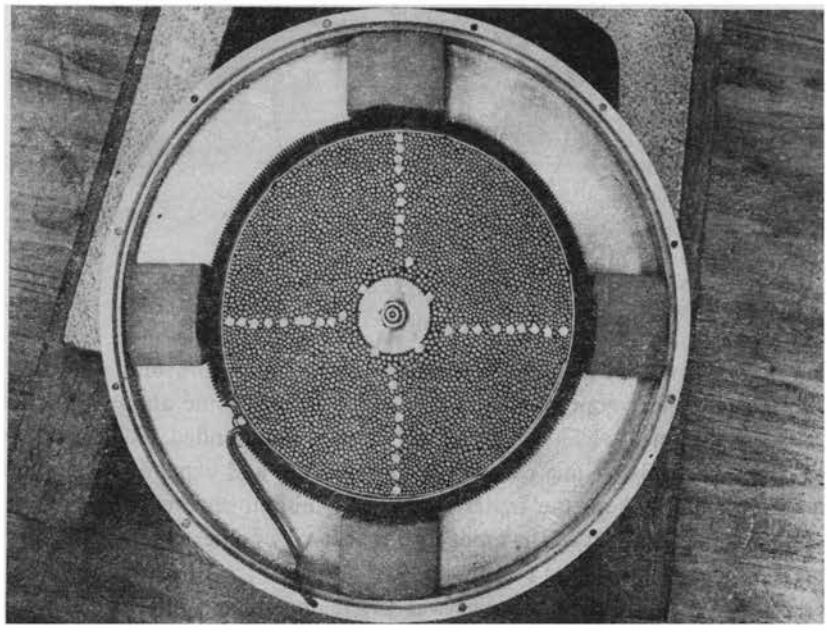

FIG. 2. The shear zone produced by a rigid rotation of the inner core; A) initial state, B) final state.

http://rcin.org.pl

2.2. Construction

After several preliminary tests we tried to use a rubber tube which allows for a unique relationship between the internal gas pressure p_t and the diameter d_t, versus the radial stress σ_r. For the outer boundary this solution was indeed applied. At the inner boundary it appeared that the circle became unstable as soon as the pressure distribution between

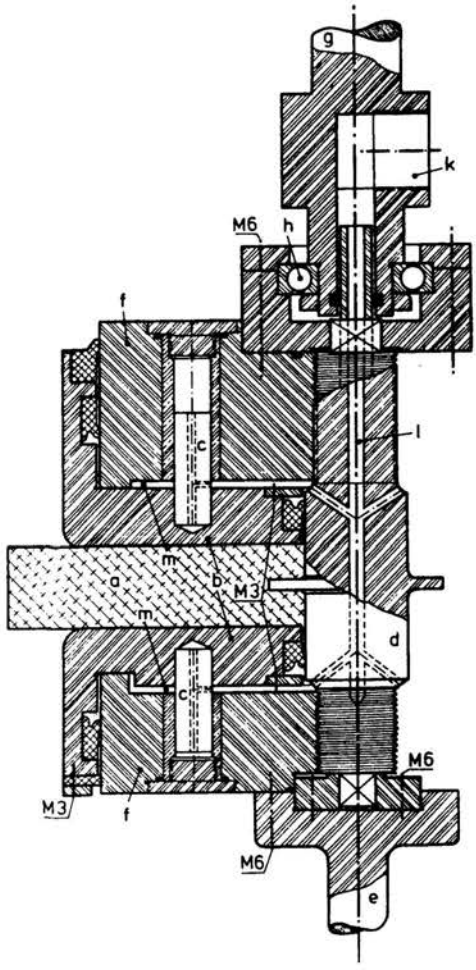

FIG. 3. Sectional view of the inner loading and measuring equipment; a) polyurethane plate, b) piston plate, c) former pin, d) shaft, e) torsional shaft, f) abutment plate, g) back-end piloting, h) ball bearing, k) delivery connection, l) bore for hydraulic oil, m) pressure chamber.

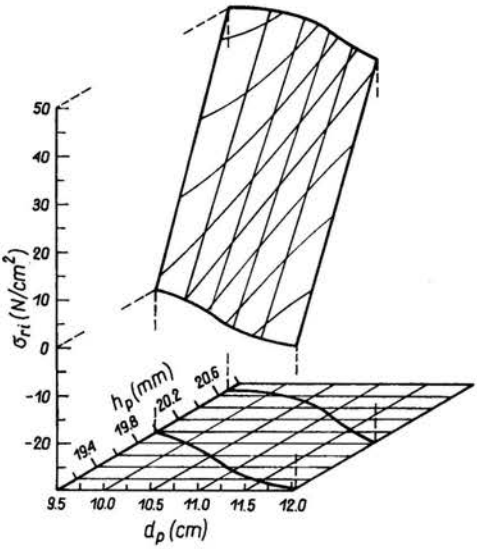

FIG. 4. The radial stress σ_{rl} as a function of the diameter d_p and the thickness h_p of the polyurethane plate.

the model material and the rubber tube underwent any perturbation like, for example deviation from the rotational symmetry. Therefore we chose the following different solution (Fig. 3): A polyurethane plate is compressed between two hydraulic head-on-acting cylinders, so that the diameter is increased. The pressure σ_{ri} between the plate and the granular material are determined by calibration tests, to depend on the actual diameter d_p and the thickness h_p of the plate (Fig. 4). The change of thickness is measured with the aid of linear variable differential transformers, the diameter by a self-made strain transformer. The shear stress τ_i at the inner boundary is transferred by means of friction from

http://rcin.org.pl

the polyurethane plate to the cylinders, and can now be measured as a torque acting onto the torsional shaft which simultaneously transfers the rotation to the inner core.

At the outer boundary r_e (Fig. 5), sheet segments transfer the shear stress τ_e by means of former pins to a rigid steel ring inside which the rubber tube is placed. The ring is supported by four flexural levers on which bonded strain gages are fixed for the purpose of displaying the value of the transferred moment. The radial normal stress σ_{re} can be won by

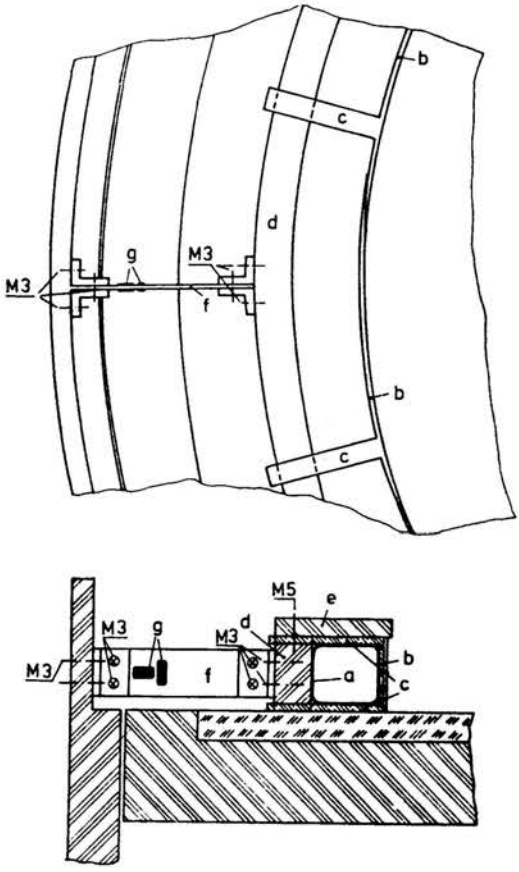

FIG. 5. The outer loading and measuring equipment; A) top view without the cover plate (e), B) sectional view; a) rubber tube, b) sheet segments, c) former pins, d) rigid steel ring, e) circular ring slab, f) flexural members, g) strain gages.

interpolating the surface of Fig. 6 if the actual diameter d_t of the rubber tube and the internal gas pressure p_t are known. Figure 7 shows a photograph of the setup.

It is possible to prescribe one of the kinematic quantities only, e.g. the radial extension u_i, as the angular velocity of the inner core $\Omega = 0.006$ r.p.m. is enforced by the invariable speed of the electromotor in combination with the transmission ratio, while the outer boundary can not be rotated. In order to control the extension u_i we use the rotation Ω as the reference input ratio. Regarding the stresses, only the radial pressure σ_{re} can be prescribed independently, i.e. by means of a blow-off valve within certain tolerances. An

http://rcin.org.pl

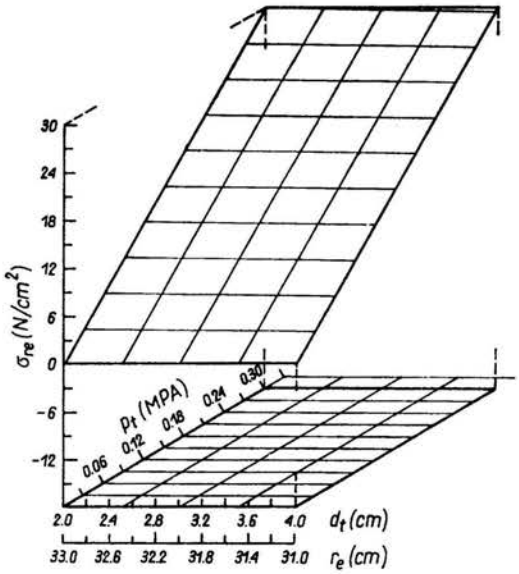

FIG. 6. The radial normal stress σ_{re} as a function of the diameter d_t and the internal gas pressure p_t of the rubber tube.

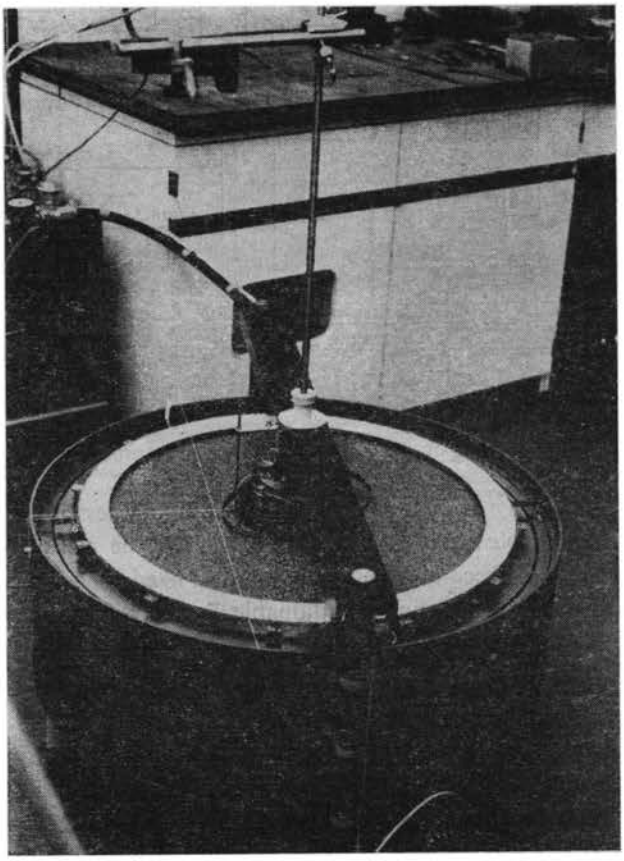

FIG. 7. Photograph of the setup.

http://rcin.org.pl

upper limit of σ_{re} is imposed by the load-carrying capacity of the torsional shalft because the shear stress τ_i increases if the normal stress σ_{re} augments, while the same kinematic boundary conditions remain unchanged.

2.3. Registering of the measured values

The measurement of the different values is controlled by a pulse generator (Fig. 8) which simultaneously releases the camera and gives a binary signal to the Sample and Hold Storage so that the actual measured quantities are kept. Besides, the scanner is caused by the printer to record the successive data via a digital voltmeter. After a fixed

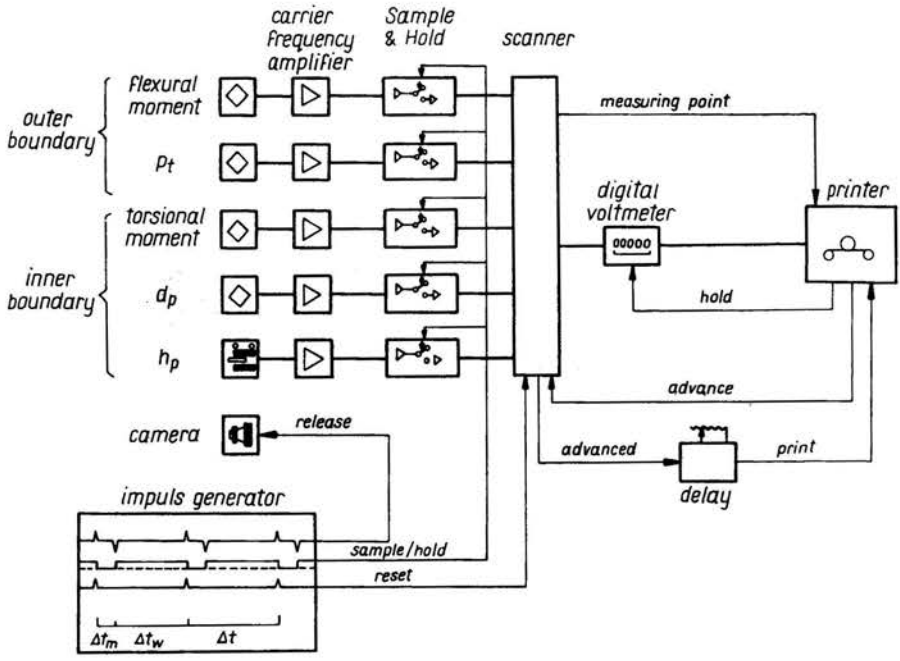

FIG. 8. Block diagram for the registering process.

time interval Δt_m — as early as possible after the printing process is finished — the pulse generator orders the Sample and Hold Storage to sample the measured quantities, and releases the camera for the second time. After another fixed time interval Δt_w this cycle starts again, until the maximal or minimal attainable diameter d_p of the polyurethane plate is reached. The interval between two successive measurements is $\Delta t = \Delta t_m + \Delta t_w$.

3. Evaluation

The plastic components of the strain increments $\Delta\varepsilon_{jk}$ are determined in the whole area starting from the measured increments of the displacements Δu and Δv along a radius vector r by means of two photographs (Fig. 9) in a stereoscopic way. In fact, stereoscopic measurements usually presume two photographs of the object in question, taken from

http://rcin.org.pl

different positions. Then it is possible to reconstruct the object three-dimensionally by relating corresponding points of the photographs. In our case we do not use two different positions, but the model material is moving. If one looks stereoscopically at two photographs taken after a short interval, the displacements look like pseudo differences in altitude. These can be analysed as a profile along the radius vector r. Besides, the two threads are reference lines of zero displacement. The scale for the evaluation is determined

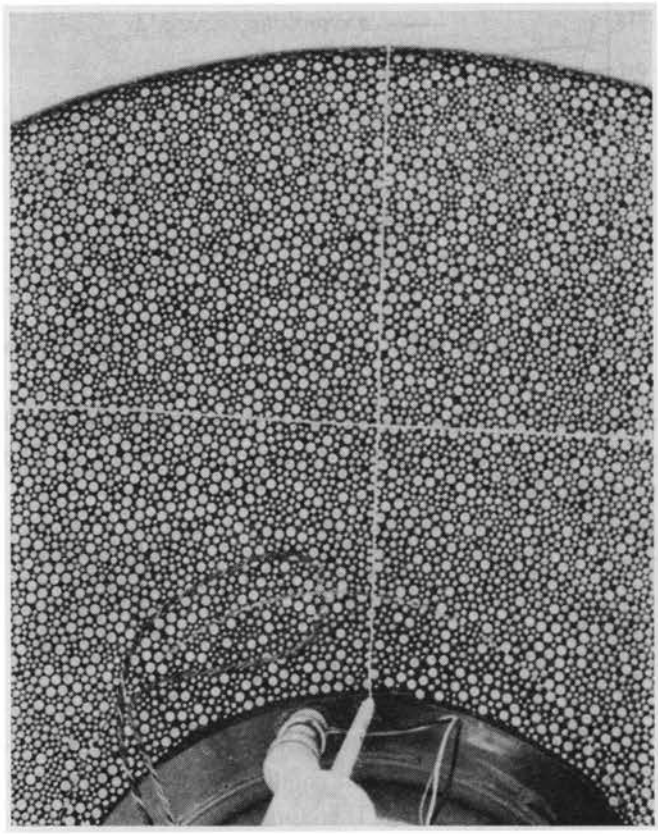

FIG. 9. Photograph used for determining the incremental displacements Δu and Δv.

by the aid of known displacements, for instance Δu_i and Δv_i. If elastic deformations are neglected one has approximately, using polar coordinates,

$$\Delta\varepsilon_{rr} = \frac{d(\Delta u)}{dr}\,,$$

$$\Delta\varepsilon_{\theta\theta} = \frac{\Delta u}{r}\,, \tag{3.1}$$

$$\Delta\varepsilon_{r\theta} = \frac{1}{2}\left(\frac{d(\Delta v)}{dr} - \frac{\Delta v}{r}\right).$$

http://rcin.org.pl

In order to obtain the derivatives $d(\Delta u)/dr$ and $d(\Delta v)/dr$ as exactly as possible, we approximate the measured values of Δu or Δv respectively, by means of smooth functions (Fig. 10) in analytical terms, and differentiate these in a closed form.

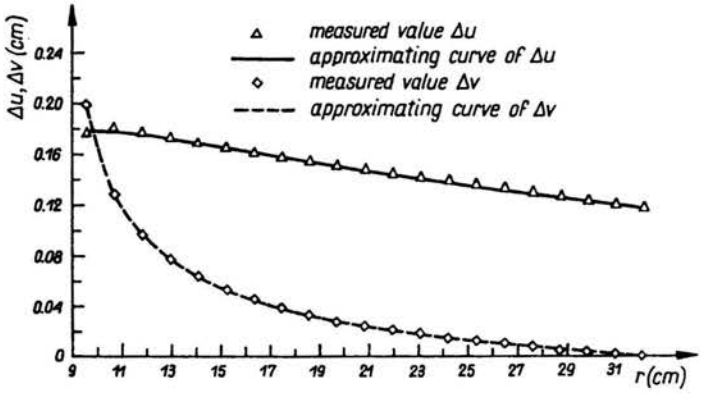

FIG. 10. Increments of the radial and circumferential displacements Δu and Δv.

Since preliminary tests show that the friction between the rodlets and the bottom plate cannot be neglected, we take account of that friction as if it would act like volume forces in the conditions of equilibrium:

$$\frac{d\sigma_r}{dr} = \frac{1}{r}(\sigma_\theta - \sigma_r) + \mu\varrho l\gamma \sin\left(\operatorname{arc\,tg}\frac{\Delta u}{\Delta v}\right),$$

$$\frac{d\tau}{dr} = -\frac{2}{r}\tau + \mu\varrho l\gamma \cos\left(\operatorname{arc\,tg}\frac{\Delta u}{\Delta v}\right). \tag{3.2}$$

Though the boundary values σ_{ri}, τ_i, σ_{re} and τ_e are being picked up during the experiments it is impossible to integrate the differential conditions of equilibrium (3.2) uniquely as any information about σ_θ is still missing. Therefore we assume:

A3: *The principal axes of stress and the increments of strain are coaxial.*

The good agreement of this assumption with reality has been shown by ROSCOE [8]. The angle α between the r-direction and the first principal axis of stress is given by

$$\operatorname{tg} 2\alpha = \frac{2\tau}{\sigma_r - \sigma_\theta}. \tag{3.3}$$

For the strain increments, it holds accordingly that

$$\operatorname{tg} 2\alpha = \frac{2\Delta\varepsilon_{r\theta}}{\Delta\varepsilon_{rr} - \Delta\varepsilon_{\theta\theta}} = \frac{\dfrac{d(\Delta v)}{dr} - \dfrac{\Delta v}{r}}{\dfrac{d(\Delta u)}{dr} - \dfrac{\Delta u}{r}}. \tag{3.4}$$

http://rcin.org.pl

Eliminating $(\sigma_\theta - \sigma_r)$ from the conditions of equilibrium (3.2), yields

$$\frac{d\sigma_r}{dr} = -\frac{2}{r}\frac{\tau}{\tan 2\alpha} + \mu\varrho l\gamma \sin\left(\operatorname{arc\,tg}\frac{\Delta u}{\Delta v}\right),$$
$$\frac{d\tau}{dr} = -\frac{2}{r}\tau + \mu\varrho l\gamma \cos\left(\operatorname{arc\,tg}\frac{\Delta u}{\Delta v}\right), \tag{3.5}$$

in which equations $\operatorname{tg} 2\alpha$ have to be substituted from Eq. (3.4). In order to find out the distribution of density, the negative copy of the photograph (Fig. 9) is put into an enlarger and the area to be analysed is scanned by a photomultiplier which reproduces exactly the

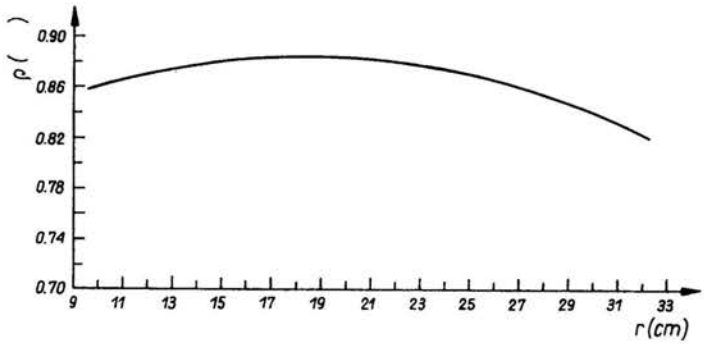

FIG. 11. Corresponding density distribution.

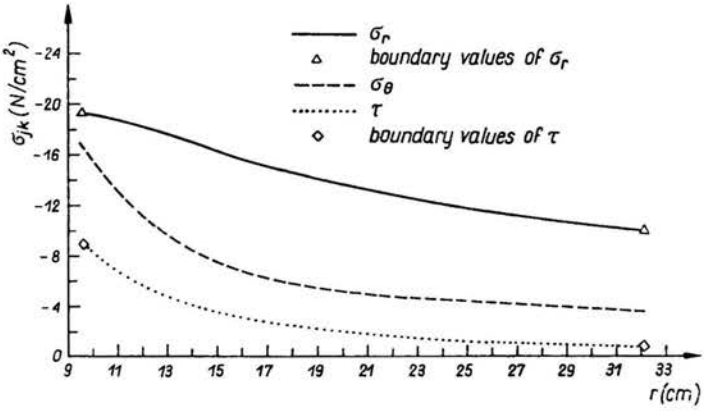

FIG. 12. Calculated stress distribution in comparison with the measured boundary values.

variation of brightness (Fig. 11). Since the negative copies do not show all the same black-white contrast, the scale has to be determined by enumerating the rodlets at least in two areas of each photograph.

Using all these informations it is now possible to integrate the differential conditions of equilibrium (3.5) with the stress boundary values σ_{ri} and τ_i given. The boundary values σ_{re} and τ_e serve as control data for the calculation. Then, a maximum deviation of four per cent between the measured and the calculated values of σ_{re} and τ_e is obtained (Fig. 12). We believe this to be a fairly good agreement.

http://rcin.org.pl

4. Results

4.1. Derivations of the constitutive equations

The abscissa of the centre σ_p and the radius σ_q of Mohr's stress circle are calculated using the determined stresses according to

$$\sigma_p = \frac{1}{2}(\sigma_r + \sigma_\theta),$$
$$\sigma_q = \frac{1}{2}|(\sigma_r - \sigma_\theta)^2 + 4\tau^2|^{1/2}, \tag{4.1}$$

and these quantities are plotted as stress points in the plane of state. Besides, the corresponding quantities taken from Mohr's circle of the strain increments

$$\Delta\varepsilon_p = \frac{1}{2}(\Delta\varepsilon_{rr} + \Delta\varepsilon_{\theta\theta}),$$
$$\Delta\varepsilon_q = \frac{1}{2}|(\Delta\varepsilon_{rr} - \Delta\varepsilon_{\theta\theta})^2 + 4\Delta\varepsilon_{r\theta}^2|^{1/2} \tag{4.2}$$

are plotted as a free vector in the corresponding stress point. Now the stress points mutually with the vectors (*) of the strain increments are consecutively arranged according to the

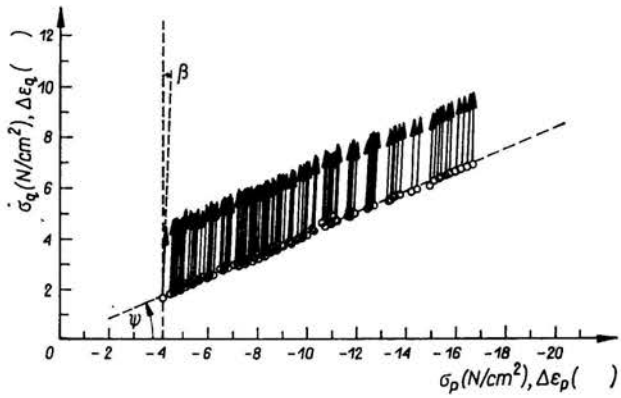

FIG. 13. Stress states on the yield limit and corresponding strain increments in the plane of state for $\varrho = 0.73$.

values of the density ϱ for all test series. Then, well-interpretable diagrams are obtained (Figs. 13 and 14). In this way a slight dependence of the yield criterion and a much larger dependence of the strain increments both on the density ϱ could be found. Furthermore, it is seen that the yield limit may be described by means of the Coulomb criterion:

$$f_o = \frac{\sigma_q}{|\sigma_p|} + \frac{\sigma_p}{|\sigma_p|}\sin\Phi - \frac{c}{|\sigma_p|}\cos\Phi = 0, \quad \sigma_p \neq 0 \tag{4.3}$$

(*) Reduced to equal lengths, as only their direction is important.

http://rcin.org.pl

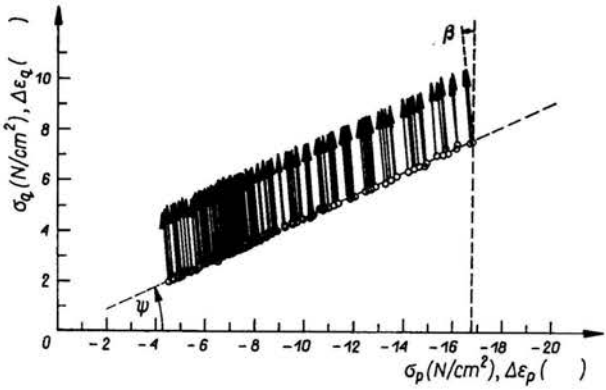

FIG. 14. Same as Fig. 13, for $\varrho = 0.82$.

in which the internal cohesion c can be neglected at least for our model material. The relation between the angle of internal friction Φ and the angle ψ in Figs. 13 and 14 is given by the equation

$$\sin\Phi = \operatorname{tg}\psi.$$

Now it appears reasonable to check flow rules which satisfy the assumption A3, so that Eqs. (3.3) and (3.4) can be derived from the constitutive equations used.

The normality condition (MISES)

$$\Delta\varepsilon_{jk} = \Delta\lambda \frac{\partial f_\sigma}{\partial \sigma_{jk}} \tag{4.5}$$

does not hold as can easily be seen from the diagram in Fig. 13. BROWN [9] maintained the normality with regard to the deviatoric quantities e_{jk}, s_{jk} of strain and stress respectively, according to

$$\Delta e_{jk} = \Delta\lambda \left(\frac{\partial f_\sigma}{\partial s_{jk}} - \partial_{jk} \frac{1}{2} \frac{\partial f_\sigma}{\partial s_{mm}} \right) \tag{4.6}$$

but has to add an additional relationship for the changes in volume as follows:

$$\Delta\varepsilon_{mm} = \Delta\lambda g(\sigma_{mm}). \tag{4.7}$$

The application of the flow rule, Eqs. (4.6) and (4.7) in combination with the approach suggested by GUDEHUS [10]

$$g(\sigma_{mm}) = -\frac{D(\sigma)}{\sigma_{mm}}, \quad \sigma_{mm} \neq 0 \tag{4.8}$$

gives a satisfactory agreement (Figs. 15 and 16) (*). D is the dilatancy function which indicates whether the volume increases ($D > 0$) or decreases ($D < 0$). The angle of dilat-

(*) It could not be examined how far Eq. (4.8) would remain correct if $\sigma_{mm} \to 0$.

http://rcin.org.pl

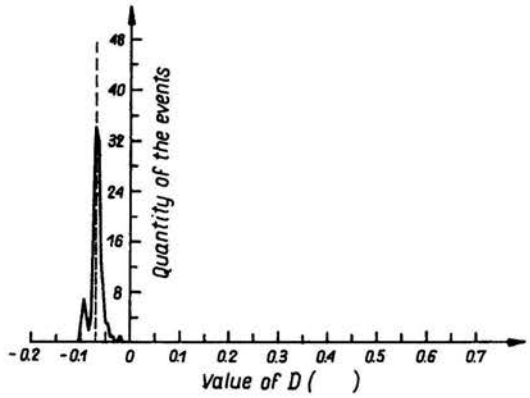

FIG. 15. Statistical analysis of the value of the dilatancy function D for $\varrho = 0.73$.

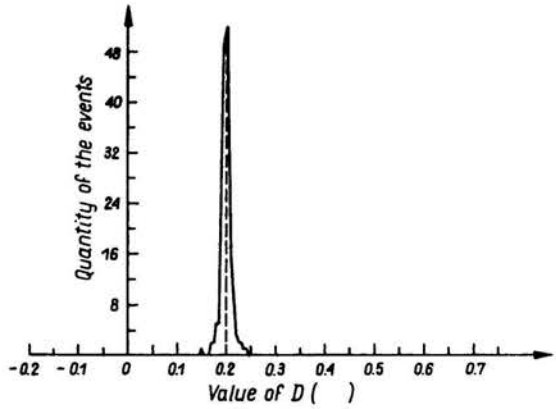

FIG. 16. Same as Fig. 15, for $\varrho = 0.82$.

ancy β (Figs. 13 and 14) between the strain increment vector and the direction of deviatoric deformation is related to D by the equation

$$D = 2\mathrm{tg}\beta. \tag{4.9}$$

As the agreement obtained in this way could, using our experiments, hardly be improved, an additional analysis was omitted which could be based on the more general flow rule suggested by POOROOSHASB [11], RADENKOVIC [12], et al.:

$$\Delta\varepsilon_{jk} = \Delta\lambda \frac{\partial\Psi_\sigma}{\partial\sigma_{jk}}. \tag{4.10}$$

After all values of the density ϱ which appear during the experiments have been analysed, it becomes evident that the angle of internal friction Φ is directly proportional to the density ϱ (Fig. 17), and that $D(\varrho)$ may be described as a polynomial of the third order (Fig. 18). As can be seen from Figs. 19 and 20, the density ϱ tends during the deformation to an asymptotic value for which a volume change does no longer happen. This "critical" density amounts approximately to $\varrho_c = 0.76$.

http://rcin.org.pl

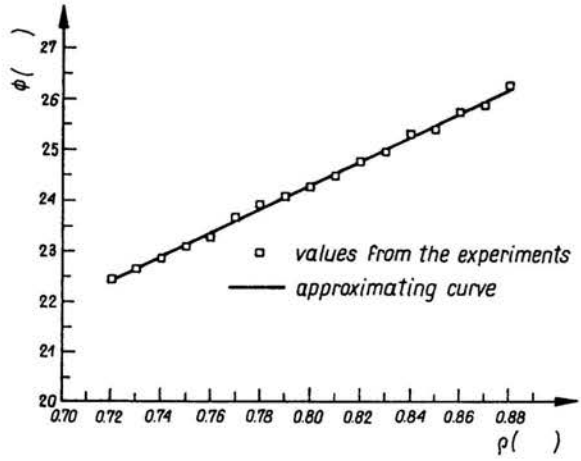

FIG. 17. The angle of internal friction Φ as a function of the relative density ϱ.

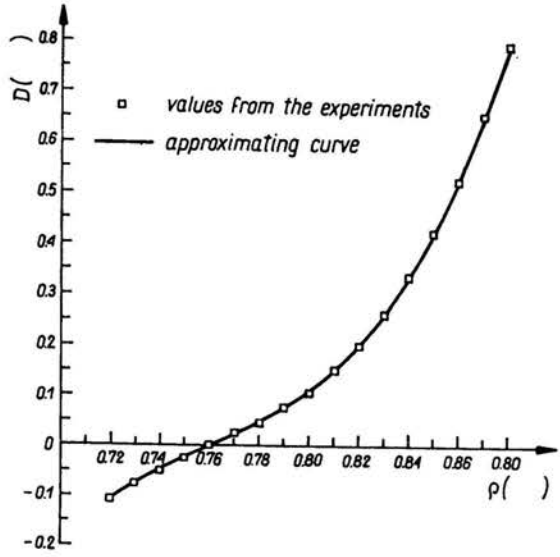

FIG. 18. The dilatancy function D dependent on the relative density ϱ.

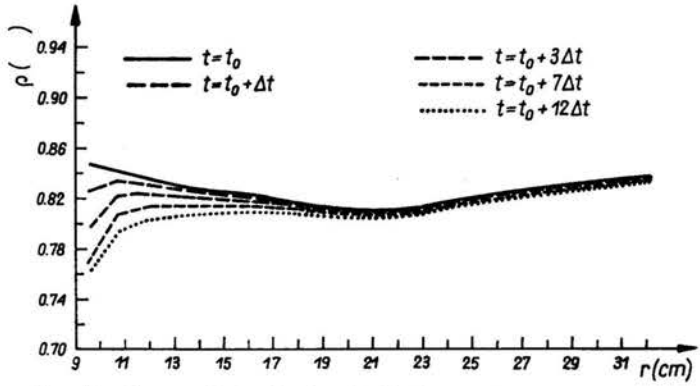

FIG. 19. Change of the density distribution during an experiment.

http://rcin.org.pl

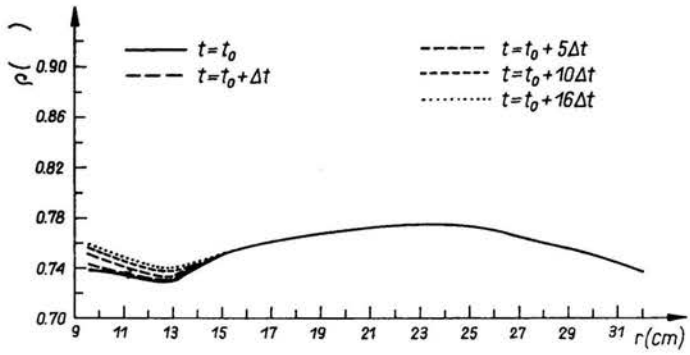

FIG. 20. Change of the density distribution for an initial state close to the critical density ϱ_c.

4.2. Another verification of the constitutive equations

In order to check the determined constitutive equations the test conditions have been changed. Whereas during the previous experiments the radial incremental displacement at the inner boundary was always positive ($\Delta u_i > 0$), i.e. the diameter of the inner core increasing, now the diameter of the inner core may also decrease ($\Delta u_i < 0$). Here the set of differential equations comprises not only the conditions of equilibrium (3.2), but also the compatibility equations (3.1) in which the strain increments have been eliminated by virtue of the flow rule in Eqs. (4.6), (4.7) and (4.8):

$$\frac{d\sigma_r}{dr} = \frac{1}{r}(\sigma_\theta - \sigma_r) + \mu\varrho l\gamma \sin\left(\operatorname{arc\,tg}\frac{\Delta u}{\Delta v}\right),$$

$$\frac{d\tau}{dr} = -\frac{1}{2}\tau + \mu\varrho l\gamma \cos\left(\operatorname{arc\,tg}\frac{\Delta u}{\Delta v}\right),$$

(4.11)

$$\frac{d(\Delta u)}{dr} = \frac{\Delta u}{r}\,\frac{\sigma_r - \sigma_\theta + \frac{D}{2}|(\sigma_r-\sigma_\theta)^2 + 4\tau^2|^{1/2}}{\sigma_\theta - \sigma_r + \frac{D}{2}|(\sigma_\theta-\sigma_r)^2 + 4\tau^2|^{1/2}},$$

$$\frac{d(\Delta v)}{dr} = \frac{\Delta v}{r} + \frac{\Delta u}{r}\,\frac{4\tau}{\sigma_\theta - \sigma_r + \frac{D}{2}|(\sigma_r-\sigma_\theta)^2 + 4\tau^2|^{1/2}}.$$

The circumferential stress σ_θ has to be substituted using the yield criterion in Eq. (4.3) by the stresses σ_r and τ.

The density distribution ϱ has to be known at least for the initial state, i.e. this distribution would have to be measured in advance, (Fig. 21), whereas the subsequent values of ϱ can be determined on the base of the volume change as obtained by the kinematics measured. With these informations it now becomes possible to integrate the set of differential equations (4.11) using the boundary values σ_{ri}, τ_i, Δu_i and Δv_i given. The boundary values σ_{re} and τ_e and the increments of the displacement Δu and Δv are used as control data (Figs. 22 and 23). In spite of the different test conditions, one obtains a fairly good agreement.

http://rcin.org.pl

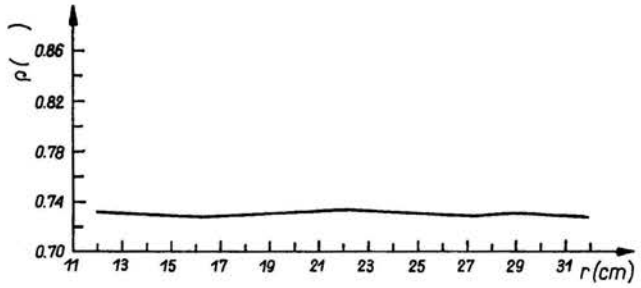

FIG. 21. Density distribution used for checking the constitutive equations ($\Delta u_i < 0$).

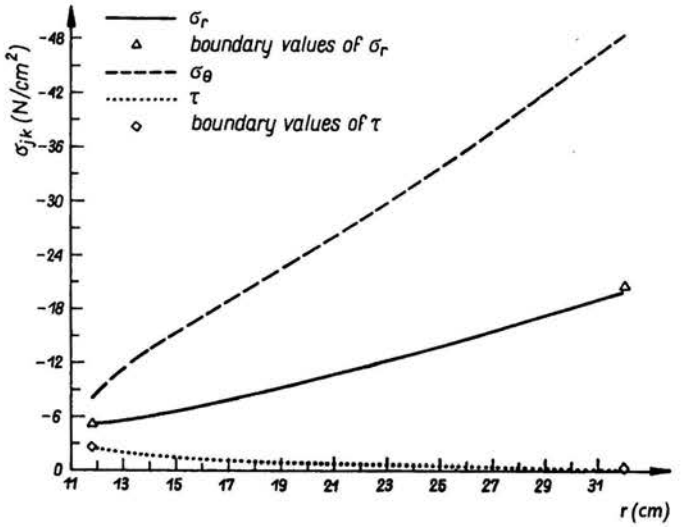

FIG. 22. Calculated stress distribution compared with the measured boundary values in the check (cp. Fig. 21).

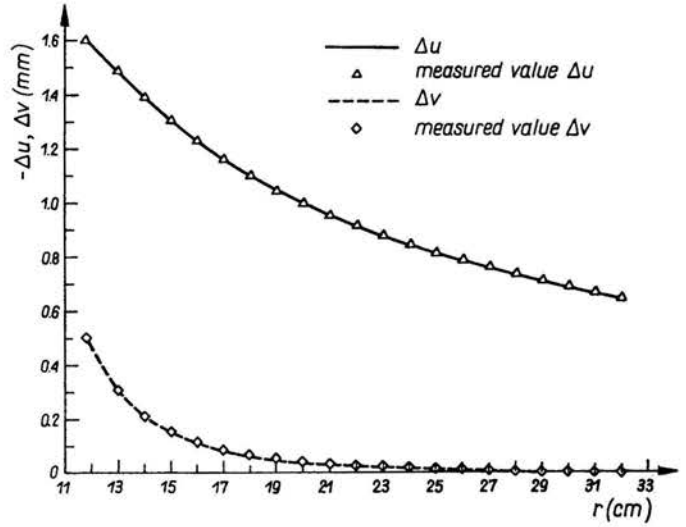

FIG. 23. Calculated increments of the displacements compared with the measured values in the check (cp. Fig. 21).

http://rcin.org.pl

5. Conclusion

It has been shown that the behaviour of our model material may be described by means of the constitutive equations (4.3), (4.6), (4.7) and (4.8). In addition, neither the velocity of deformation nor the rotation of grains show a significant feedback to the stress-displacement behaviour of this model material; thus basic assumptions (Ch. 1) seem to be justified. Therefore it appears reasonable to advance the design of the setup in such a way that any arbitrary granular material like sand, for example, can be analysed.

6. Acknowledgment

The authors are higly indepted to Mr. W. Ditscher, Mr. W. Mayer, Mr. R. Sikor, Mr. H. Weber and Mr. J. Zachmann for their support in developing the experimental and electronic device.

References

1. J. A. PEARCE, *A truly triaxial machine for testing clays*, Colloquium on Mechanical Properties of Granular Media, 95–110, Karlsruhe 1969.
2. M. GOLDSCHEIDER and G. GUDEHUS, *Rectilinear extension of dry sand, testing apparatus and experimental results*, Proceedings 8th Intern. Conf. Soil Mech. Found. Eng., I/21, 143–149, Moskau 1973.
3. F. HARTMANN, *Beitrag zur Theorie des Scherversuches*, Colloquium on Mechanical Properties of Granular Media, 125–174, Karlsruhe 1969.
4. G. GUDEHUS, *Gedanken zur Statististischen Bodenmechanik*, Bauingenieur, 43, 320–326, 1968.
5. H. M. HORN and D. U. DEERE, *Frictional characteristics of minerals*, Geotechnique, **12**, 319–335, 196
6. G. SCHNEEBELI, *Une analogie mécanique pour l'étude de la stabilité des ouvrages en terre a deux dimensions*, Proceedings Int. Soil Mech., 228–233, London 1957.
7. K. H. ROSCOE, *The influence of strains in soil mechanics*, Geotechnique, **20**, 129–170, 1970.
8. K. H. ROSCOE, *Some results of tests in the latest model of the simple shear apparatus and new biaxial apparatus*, Colloquium on Mechanical Properties of Granular Media, 62–94, Karlsruhe 1969.
9. E. H. BROWN, *A theory for mechanical behaviour of sand*, Proceedings 11th Intern. Congr. Appl. Mech., 183–191, München 1964.
10. G. GUDEHUS, *Elastic-plastic constitutive equations for dry sand*, Arch. Mech. Stos., **24**, 396–402, 1972.
11. H. B. POOROOSHASB et al., *Yielding and flow of sand in triaxial compression*, Canad. Geotechn. Journ., III, 179–190, 1966; IV, 376–397, 1967.
12. D. RADENKOVIC, *Theorie des charges limites: extension a la mécanique des sols*, Seminaire de plasticité (Ecole Polytechnique), Paris Publ. Scientifiques et Techniques du Ministere de l'Air, N.T. 116, 129–142, 1961.

FACHBEREICH BAUTECHNIK
DER GESAMTHOCHSCHULE WUPPERTAL, BRD
and
LEHRSTUHL A FÜR MECHANIK
DER TECHNISCHEN UNIVERSITÄT MÜNCHEN, BRD.

Received March 24, 1977.

http://rcin.org.pl